AIIM

Association for Information and Image Management

1100 Wayne Avenue, Suite 1100
Silver Spring, Maryland 20910

301/587-8202

Centimeter

Inches

MANUFACTURED TO AIIM STANDARDS
BY APPLIED IMAGE, INC.

1 of 1

Evolution of Turbulent Fields in Explosions

A.L. Kuhl and J.B. Bell
Lawrence Livermore National Laboratory
El Segundo, CA

R.E. Ferguson, K.-Y. Chien, J.P. Collins and M.-L. Lyons
Naval Surface Warfare Center, White Oak Detachment
Silver Spring, MD

Abstract

Explosions always contain turbulent mixing regions, e.g.: boundary layers, shear layers, wall jets and unstable interfaces. The inherent unsteadiness of turbulent mixing in explosions, and the lack of sufficient data, pose insurmountable difficulties for turbulence modeling of such flows. Proposed here is a direct numerical simulation approach—where the three-dimensional (3-D) conservation laws are integrated via a high-order Godunov method. Adaptive Mesh Refinement (AMR) is used to capture the convective mixing processes on the computational grid. Then, an azimuthal-averaging operator is applied to the 3-D solution—in order to extract the instantaneous mean and fluctuating components of the turbulent field. As an illustration, this methodology is applied to the numerical simulation of the turbulent wall jet and dusty boundary layer flow induced by a point explosion above a ground surface. Principal results include the evolution of the turbulent velocity field near the surface. During the wall jet phase, the mean profiles resemble our previous two-dimensional calculations, while the velocity fluctuation profiles and Reynolds stress profiles are qualitatively similar to measurements of self-preserving wall jets. During the boundary layer phase, the mean velocity profile evolved with time, e.g.: initially it agreed with measurements of a dusty boundary layer behind a shock; at intermediate times it resembled the dusty boundary layer profiles measured in a wind tunnel; while at late times, it approached a 1/7 power-law profile. Velocity fluctuation profiles were qualitatively similar to those measured for a turbulent boundary layer on a flat plate. The methodology can be used to predict the evolution of other turbulent fields such as dust clouds, axisymmetric jets, fireball instabilities, and dusty boundary layers in shock tube and wind tunnel flows.

MASTER

1. Introduction

Explosions always contain embedded turbulent mixing regions, for example: boundary layers, shear layers, wall jets, and unstable interfaces. There are two approaches that can be used for numerical calculations of such turbulent flows, namely, turbulence modeling or direct numerical simulation. Let us first contrast the strengths and weaknesses of each approach.

Turbulence models all begin by averaging the conservation laws. In physics this is known as the mean-field approximation, which works well if the fluctuations are always small compared to the mean values. However, as pointed out by Chorin (1975), the equations of fluid dynamics are nonlinear, and the integration of the averaged equations does not equal the average of the integrated equations. This implies that the turbulence model equations are not predictive (i.e., they cannot accurately forecast turbulent flows which lack a significant data base). The inherent unsteadiness of turbulent mixing in explosions poses a particularly difficult challenge in this regard. Hence, for this class of flows, one must resort to other approaches which are not tied to the limitations of integrating the averaged equations.

Due to recent advances in computational power and improvements in numerical algorithms (e.g., nonlinear monotone schemes and adaptive mesh refinement), it is now feasible to perform direct numerical simulations of three-dimensional (3-D) turbulent flows. Recent studies by Bell and Marcus (1992), and Oran and Boris (1993) have shown that time-dependent solutions of the 3-D conservation laws exhibit all the properties associated with turbulent flows—including the Kolmogorov energy spectrum with a power-law slope of -5/3—if enough grid resolution is used. The problem then becomes: how can one extract order from this turbulent 3-D solution? For example, in many engineering applications one is primarily interested in the mean flow. Clearly, the way to construct the mean of nonsteady flows is by ensemble averaging—but it is impractical to perform hundreds of 3-D calculations.

To solve such dilemmas, this paper presents a methodology for evaluating averages of turbulent fields in symmetric explosions from a single direct numerical simulation. As an illustration, this methodology is then applied to a 3-D simulation of the dusty boundary layer induced by an explosion above a ground surface.

2. Averaging Methodology

We begin with a turbulent flowfield $\phi\,(x, y, z, t)$ derived from a direct integration of the 3-D conservation laws. We assume that the explosion is initially spherical (i.e., no jetting). Then it is reasonable to expect that the laminar flowfield outside the turbulent mixing region is azimuthally symmetric. Take advantage of this unlying symmetry and sample the solution at fixed azimuths $\theta_k = 2\pi k/K$ in a cylindrical coordinate system:

$$\phi\ (x, y, z, t) \longrightarrow \phi\ (r, z, \theta_k, t)$$

This forms a set

$$\{\phi\,(\theta_1), \phi\,(\theta_2) \ldots\ldots \phi\,(\theta_K)\}$$

where the dependence on other variables has temporarily been suppressed for clarity. One can view this set as K realizations of the turbulent flow, in other words, an ensemble.

If this ensemble is statistically representative, then one can think of forming averages of the turbulent flow. In particular, divide the flow field ϕ into a mean component $\overline{\phi}$ and a fluctuating component ϕ':

$$\phi = \overline{\phi} + \phi' \tag{1}$$

such that $\overline{\phi'} = 0$. Let us define an azimuthal averaging operator $\mathcal{A}$:

$$\mathcal{A}\{\ \} = \frac{1}{K}\sum_{k=1}^{K}\{\ \} \tag{2}$$

Then application of the averaging operator to ϕ extracts the mean component of the flow:

$$\overline{\phi}(r,z,t) = \mathcal{A}\{\phi\} = \frac{1}{K}\sum_{k=1}^{K}\phi(r,z,\theta_k,t). \tag{3}$$

while application of the averaging operator to $(\phi')^n$ extracts the nth moments of the flow:

$$\overline{(\phi')^n} = \mathcal{A}\left\{(\phi')^n\right\} = \frac{1}{K}\sum_{k=1}^{K}\left[\phi(r,z,\theta_k,t) - \overline{\phi}(r,z,t)\right]^n \tag{4}$$

and the root-mean-squared (r.m.s.) fluctuations:

$$\phi'(r,z,t) = \sqrt{\overline{(\phi')^2}}\ . \tag{5}$$

The above relations may be used for scalars. In order to calculate the Reynolds stress tensor τ_{ij}, one must consider the velocity field $u_i(r,z,\theta_k,t)$. Then, application of the averaging operator to $u_i'u_j'$ extracts the Reynolds stress:

$$\begin{aligned}\tau_{ij}(r,z,t) &\equiv \mathcal{A}\left\{u_i'u_j'\right\} \\ &= \frac{1}{K}\sum_{k=1}^{K}\left[u_i(r,z,\theta_k,t) - \overline{u_i}(r,z,t)\right]\left[u_j(r,z,\theta_k,t) - \overline{u_j}(r,z,t)\right]\end{aligned} \tag{6}$$

while the r.m.s. velocity fluctuations are related to the diagonal components of the Reynolds stress by:

$$u_i'(r,z,t) = \sqrt{\tau_{ii}}\ . \tag{7}$$

Thus, by storing the complete flowfield at a few times t^n, this methodology allows one to visualize the evolution of the azimuthally-averaged flow. For example, one can make two-dimensional (2-D) contour plots of the mean flow $\overline{\phi}(r,z,t^n)$ and r.m.s. fluctuations $\phi'(r,z,t^n)$ at various times. In addition, by selecting fixed ground ranges r_l, one can display the evolution of the boundary layer profiles: $\overline{u_i}(r_l,z,t^n), u_i'(r_l,z,t^n)$ and $\tau_{ij}(r_l,z,t^n)$. Examples of these will be presented in subsequent sections.

3. The Problem

The problem considered here is the turbulent boundary layer flow induced by a 37-KT point explosion detonated 203 meters above a ground surface that had an initial loose dust layer (see Figure 1). While much is known about blast wave reflections from ideal surfaces (e.g., through gas dynamic calculations of Colella et al., [1986] and laboratory experiments of Reichenbach et al., [1992]), much less is known about the details of the boundary layer flow from explosions over real surfaces. One of the reasons is that the flow is considerably more complex (see Figure 1).

For a point explosion over a ground surface, thermal radiation from the fireball heats the air near the surface, creating a thermal layer TL ahead of the shock front. The blast wave propagates faster in the high-sound-speed layer, generating an outrunning precursor shock P. Gas from the main blast wave fills in the flow behind the precursor, forming a turbulent wall jet (Figure 2). At the same time, vorticity is generated by baroclinic effects (i.e., pressure gradients interacting with oblique density gradients). For example, shock interactions with the dust bed create a boundary layer along the surface, while shock interactions with the thermal layer create a vortex sheet that passes up and over the top of the wall jet. These shear layers roll-up and interact, forming the turbulent wall jet flow seen in Figure 2. Dust scouring occurs because the vortex tubes entrain mass from the fluidized bed and mix it throughout the boundary layer.

The details of modeling the dusty flow have been published elsewhere (Kuhl et al., 1993). The primary assumption was that the dust and air are in thermal and mechanical equilibrium (however, nonequilibrium models may also be used; see Collins et al., 1994). This results in the 3-D conservation laws of gasdynamics for the mixture. These are augmented a convection equation for the dust mass concentration. The conservation laws are integrated numerically with a second-order Godunov algorithm (Colella and Glaz, 1985). Adaptive Mesh Refinement (AMR) was used to calculate the convective mixing processes on the computational grid. Three levels of mesh refinements were used: grid 1 defined the computational domain of 2000 m^3 (Δ_1 = 24 m); grid 2 was used to capture the shock waves (Δ_2 = 6 m); while grid 3 followed the dusty wall jet flow (Δ_3 = 1.5 m). The problem was run to a time of 2 seconds, which took about 60 CPU hours on the Cray Y-MP.

A 3-D visualization of the turbulent wall jet and dusty boundary layer flow is depicted in Figure 3. Three-dimensional effects are quite evident, for example: streamwise vortex structures (Görtler vortices) in the boundary layer region (view a) and hairpin structures in the wall jet flow (view b). The question is: does this chaotic mixing layer possess smooth mean profiles that are similar to other well-documented turbulent flows? This question is explored in the next two sections.

4. Wall Jet Profiles

The azimuthal-averaging operator was applied to u_r in order to determine the mean streamwise velocity $\bar{u}_r(r,z,t) = \mathcal{A}\{u_r\}$. The time evolution of the resulting mean radial velocity profiles is depicted in Figure 4 for two fixed ranges (r = 600 m and 700 m). The profiles exhibit the characteristic wall jet shape: velocities are zero in the fluidized bed (z < 17 m); they reach a maximum value in the middle of the jet ($z \simeq 40$ m); and then decay to the freestream flow as one moves away from the surface. For the first time we can actually visualize the temporal evolution of the mean profiles. For example, at 600 meters the wall jet grows in strength to reach a maximum velocity of about 800 m/s at t = 0.60 s; later it relaxes to a boundary layer flow (u_r < 200 m/s) after the wall jet

has passed over this station. Similar trends are seen at 700 meters, but the peak values are somewhat smaller (~600 m/s) due to blast wave decay with range; maximum velocities in the boundary layer are less than 50 m/s at late times (t = 1.45 s).

In order to compare the present results with other wall-jet flows, the velocities were non-dimensionalized by the instantaneous maximum mean velocity $u_m(t)$, and then the profiles

$$\bar{u}_i / u_m = f_i(r, \eta_J, t) \tag{8}$$

were scaled with the wall jet similarity variable η_J (Bajura and Catalano, 1975):

$$\eta_J = (z - z_o) / (z_* - z_o) \tag{9}$$

where

$z_o(t)$ = height of the fluidized bed (i.e., where $\bar{c}$ = 2/3),
$z_*(t)$ = height of free shear layer (i.e., where $\bar{u} = u_*$), and
$u_* = (u_m + u_\infty)/2$.

The fiducial z_o removes the flow in the fluidized bed from further consideration. Thus the fluidized bed is an artifice that is used to allow dust entrainment into the flow in a natural way that mimics the fluid mechanics (i.e., without imposing some artificial dust injection model), but is not part of the boundary layer flow per se. The wall jet then scales with the height of the free shear layer, δ_{FSL}:

$$\delta_{FSL}(t) = z_*(t) - z_o(t). \tag{10}$$

The mean velocity profiles in the precursor wall jet are depicted in Figure 5 for the same two ground ranges (r = 600 m and 700 m). The azimuthal-averaging procedure gives smooth, well-behaved profiles. The scaling technique seems to collapse the radial velocity profiles (Figures 5a and 5d) into a shape that is characteristic of other wall-jet flows (Launcher and Rodi, 1981; Wygnanski et al., 1992). Nevertheless, the profile shape changes somewhat over time, indicating that the wall jet is not truly self-similar. (Of course, there is no reason to expect that the profile shape would be independent of time for such a decaying blast wave problem.)

The mean vertical velocities (Figures 5b and 5e) oscillate about zero $(-0.1 < \bar{u}_z / u_m < 0.1)$ in response to the rotational structures in the wall jet. At later times (corresponding to symbol x) the flow direction is toward the surface as gas from the main blast wave rushes in to support the wall jet flow. Mean azimuthal velocities (Figures 5c and 5f) are small—typically a few percent of u_m.

Previously, we had performed detailed two-dimensional (2-D) calculations of this same precursor wall jet flow (Kuhl et al., 1993). In that case we *time-averaged* the solution in wall jet coordinates (Equation 9) to evaluate the mean-flow profiles. Note that with that technique, one produces a single profile that is characteristic of the mean flow at that ground range. For comparison purposes, the 2-D results have been plotted in Figure 5 as the solid curves labeled 2-D. Clearly, the 2-D mean profiles are qualitatively similar to the present 3-D results; however, only the 3-D calculation allows one to properly evaluate the temporal evolution of the profiles.

Evolution of the corresponding turbulent velocity fluctuation profiles

$$u_i' / u_m = g_i(r, \eta_J, t) \tag{11}$$

are depicted in Figure 6 for the same two ground ranges. For comparison, measured profiles for a 2-D, self-preserving, clean wall jet (Launder and Rodi, 1981) are included as dashed-line curves. Profiles of the radial (or streamwise) component of the velocity fluctuations are shown in Figures 6a and 6d. They exhibit a bimodal distribution, qualitatively similar to the experimental profiles: velocity fluctuations peak in the boundary layer $(\eta_J \simeq 0.2)$ and then again in the free shear layer $(\eta_J \simeq 1)$ portion of the jet. Values range from 20 to 30 percent of u_m. The second peak (near $\eta_J = 1$) disappears at late times (time symbol x) as the flow relaxes to a boundary layer flow after the wall jet has passed the considered ground range.

Evolution of the vertical component of the turbulent velocity fluctuations are depicted in Figures 6b and 6e. The profiles exhibit a single-hump shape, qualitatively similar to the experimental profiles. Values range from 10 to 20 percent of u_m.

Evolution of the azimuthal component of the turbulent velocity fluctuation profiles are depicted in Figures 6c and 6f. They exhibit a bimodal shape—with a peak in the boundary layer $(\eta_J \simeq 0.2)$ and a second peak in the free shear layer $(\eta_J \simeq 1)$—that is qualitatively similar to the experimental profiles. Values range from 10 to 20 percent of u_m. The second peak disappears at late times (time symbol x) as the flow relaxes to a boundary layer flow after the wall jet has passed the considered ground range.

For comparison purposes, results from the previous 2-D simulation of this problem are presented in Figure 6 as the solid curves labeled 2-D. The 2-D profiles are qualitatively similar to the present 3-D results, but the peak values are too large—typically by a factor of 1.5 to 2. This is a result of the 2-D flow approximation where the turbulent fluctuations are shared among two degrees of freedom versus the three degrees of freedom found in real turbulent flows.

Evolution of the corresponding turbulent Reynolds stress profiles are depicted in Figure 7 for the same two ground ranges. The radial-vertical component $u_r'u_z'$ (Figure 7a and 7d) has a negative peak in the boundary layer $(\eta_J \simeq 0.2)$ and a positive peak in the free shear layers $(\eta_J \simeq 0.8)$—as is typical of measured wall jet profiles. Profiles of other components of the calculated turbulent Reynolds stress are more erratic. Apparently one needs a bigger spectrum of samples to get smooth, well-behaved profiles for these components. Unfortunately there are no experimental measurements to guide further assessment of these profiles.

In summary, the preceding figures suggest that this blast wave wall jet is not self-similar (or self-preserving). Instead the profiles evolve over time, and finally relax to a boundary layer flow—whose properties will be examined in the next section.

5. Boundary Layer Profiles

In order to compare the present results with other boundary layer flows, the mean velocity profiles:

$$\bar{u}_i / u_m = F_i(r, \eta_{BL}, t) \tag{12}$$

were rescaled with the boundary layer similarity variable, η_{BL}:

$$\eta_{BL} = (z - z_o) / (z_{BL} - z_o) \tag{13}$$

where $z_{BL}(t)$ denotes the boundary layer height (i.e., where $\bar{u}_r = 0.99\ u_m$). This assumes that the profiles scale with the boundary layer velocity thickness, δ_{BL}:

$$\delta_{BL}(t) = z_{BL}(t) - z_o(t). \tag{14}$$

Again, the fiducial z_o removes the fluidized bed from the boundary layer analysis.

The evolution of the mean velocity profiles is depicted in Figure 8 for the same two ground ranges (r = 600 m and 700 m). For comparison purposes, various experimental profiles are included as dashed lines: curves labeled NS and WT represent the dusty boundary layer profiles measured behind a normal shock (Batt et al., 1988) and in a steady-flow wind tunnel (Batt et al., 1993), respectively; while curves labeled FP denote the clean turbulent layer on a flat plate (Klebanoff, 1955). Clearly, the mean radial velocity profile changes with time (Figures 8a and 8d). During the wall jet phase (symbols ❑, ○, Δ, and +), the profiles resemble a dusty boundary layer behind a shock; at intermediate times, the profiles resemble the dusty boundary layer in a wind tunnel; while at late times, the profiles approach the clean flat plate case. In effect what happens is that the vortex tubes in the boundary layer entrain dusty mass from the fluidized bed—thereby continuously decreasing its mean density (see Appendix A for more details). The corresponding mean densities in the bottom of the boundary layer also decrease with time—which allows the mean velocities in the bottom of the boundary layer to creep up toward the clean flat plate values.

The mean vertical velocity profiles are presented in Figures 8b and 8e. Vertical velocities are essentially zero during the wall jet phase, but then expand upward during the boundary layer phase as a result of the divergence of the blast wave flow. Mean azimuthal velocities remain near zero at all times.

Evolution of the corresponding turbulent velocity fluctuation profiles:

$$u_i' / u_m = G_i(r, \eta_{BL}, t) \tag{15}$$

are presented in Figure 9 for the same two ground ranges (r = 600 m and 700 m). The azimuthal averaging operator is adequate to give smooth, well-behaved profiles. The radial velocity fluctuations grow with time, and reach a peak value of 30 percent of u_m during the wall-jet phase. Then they relax to a profile that is relatively independent of time, with a peak value at the bottom of the boundary layer of about 20 percent of u_m. This profile is about a factor of two greater than the clean flat plate case.

Similar trends are found in the vertical and azimuthal velocity fluctuation profiles. At late times, they relax to a time-independent profile. Near $\eta_{BL} = 0$, azimuthal fluctuations are larger than vertical fluctuations (0.12 u_m versus 0.08 u_m , respectively). This is the same trend as observed for a turbulent boundary layer on a flat plate (see dashed curves) where $(u_\theta')\max \simeq 1.5(u_z')\max$.

The turbulent Reynolds stress profiles are depicted in Figure 10, using boundary layer scaling. As in Figure 7, the profiles are somewhat erratic. Apparently one needs a larger spectrum of samples to get smooth, well-behaved profiles for these components.

8. References

1. Bajura, R.A. and Catalano, M.R., (1975) "Transition in a two-dimensional plane wall jet," *J. Fluid Mech.*, **70**, pp. 773-799.

2. Bell, J.B. and Marcus, D.L. (1992) "Vorticity intensification and transition to turbulence in the 3-D Euler equations," *Comm. Math. Phys.*, **147**, 374-394.

3. Berger, M.J. and Colella, P. (1989) "Local Adaptive Mesh Refinement for shock hydrodynamics," *J. Comput. Phys.*, **82**, 64-84.

4. Chorin, A.J., (1975) "Lectures on Turbulence Theory," *Publish or Perish, Inc., Boston* (vid. esp. Chapter I-3, "An example of the perils of dishonesty," pp. 21-23).

5. Colella, P. and Glax, H.M. (1985) "Efficient solution algorithms for the riemann problem for real gases," *J. Comput. Phys.*, **59**, 264-289.

6. Launder, B.E. and Rodi, W. (1981) "Turbulent wall jet", *The 1980-81 AFOSR-HTTM-Stanford Conference on Complex Turbulent Flows: Comparison of Computation and Experiment*, Vol. I, Mech. Engin. Dept., Stanford University, Stanford, CA, pp. 434-451.

7. Klebanoff, P.S. (1955) "Characteristics of Turbulence in a Boundary Layer with Zero Pressure Gradient," *NACA Report 1247*.

8. Kuhl, A.L. et al., (1993) "Turbulent wall jet in a blast wave precursor," *Japanese National Symposium on Shock Wave Phenomena*, edited by K. Takayama, Tohoku Print, Sendai, Japan (in press). Also available as a preprint Lawrence Livermore National Laboratory, Livermore, CA UCRL-JC-112713.

9. Oran, E.S. and Boris, J.P. (1993) "Computing Turbulent Shear Flows—A Convenient Conspiracy" (submitted to *Computer in Physics*).

10. Wygnanski, I., Katz, Y. and Horex, E., (1992) "Applicability of scaling laws to the turbulent wall jet," *J. Fluid Mech.*, 234, pp. 669-690.

Acknowledgments

Work performed under the auspices of the U.S. Department of Energy by the Lawrence Livermore National Laboratory under Contract Number W-7405-ENG-48. Also sponsored by the Defense Nuclear Agency under DNA IACRO #93-818, and Work Unit 00003.

Figure Captions

Figure 1. Explosion over a dusty surface (t = 1 s).

Figure 2. Cross-sectional view of the turbulent wall jet flow (t = 0.73 s).

Figure 3. Three-dimensional visualization of the turbulent wall jet and dusty boundary layer flow at 1.68 s: (a) oblique view of the dust concentration; (b) vorticity magnitude, viewed looking toward ground zero.

Figure 4. Evolution of the mean radial velocity profile versus time: (a) 600 m; (b) 700 m..

Figure 5. Mean velocity profiles in a precursor wall jet at 600 m (a - radial, b - vertical, c - azimuthal) and 700 m (d, e, f). Solid line denotes previous 2-D calculation (Kuhl et al., 1993).

Figure 6. Velocity fluctuation profiles in a precursor wall jet at 600 m (a - radial, b - vertical, c - azimuthal) and 700 m (d, e, f). Solid line denotes previous 2-D calculation (Kuhl et al., 1993).. Dashed lines denote measurements of a self-preserving 2-D clean wall jet (Launder and Rodi, 1981).

Figure 7. Reynolds stress profiles in a precursor wall jet at 600 m (a - radial, b - vertical, c - azimuthal) and 700 m (d, e, f). Solid line denotes previous 2-D calculation (Kuhl et al., 1993).. Dashed lines denote measurements of a self-preserving 2-D clean wall jet (Launder and Rodi, 1981).

Figure 8. Mean velocity profiles in the boundary layer at 600 m (a - radial, b - vertical, c - azimuthal) and 700 m (d, e, f). Curves labeled NS and WT represent the dusty boundary layer profiles measured behind a normal shock (Batt et al., 1988) and in a wind tunnel (Batt et al., 1993), respectively, while curves labeled FP represent the turbulent boundary layer on a clean flat plate.

Figure 9. Velocity fluctuation profiles in the boundary layer at 600 m (a - radial, b - vertical, c - azimuthal) and 700 m (d, e, f). Dashed line represents measurements of a turbulent boundary layer on a clean flat plate (Klebanoff, 1955).

Figure 10. Reynolds stress profiles in the boundary layer at 600 m (a - radial, b - vertical, c - azimuthal) and 700 m (d, e, f). Dashed line represents measurements of a turbulent boundary layer on a clean flat plate (Klebanoff, 1955).

Figure . Mean flow profiles in a precursor wall jet: the 3-D calculation (a - density, b - pressure, c - dynamic pressure) compared with the previous 2-D calculation (d, e, f).

Figure . Fluctuation profiles in a precursor wall jet: the 3-D calculation (a - density, b - pressure, c - dynamic pressure) compared with the previous 2-D calculation (d, e, f).

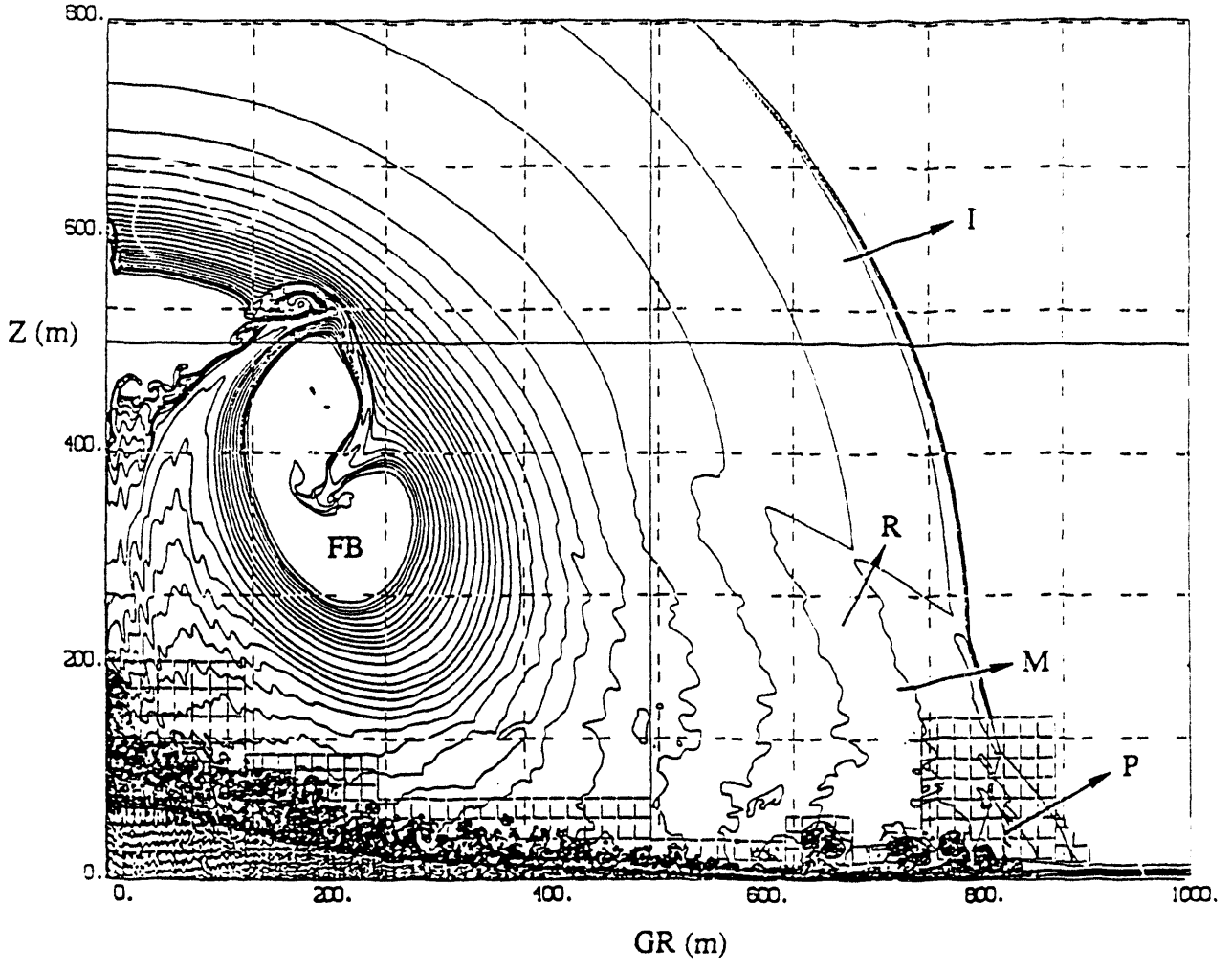

Figure 1. Explosion over a dusty surface (t = 1 s).

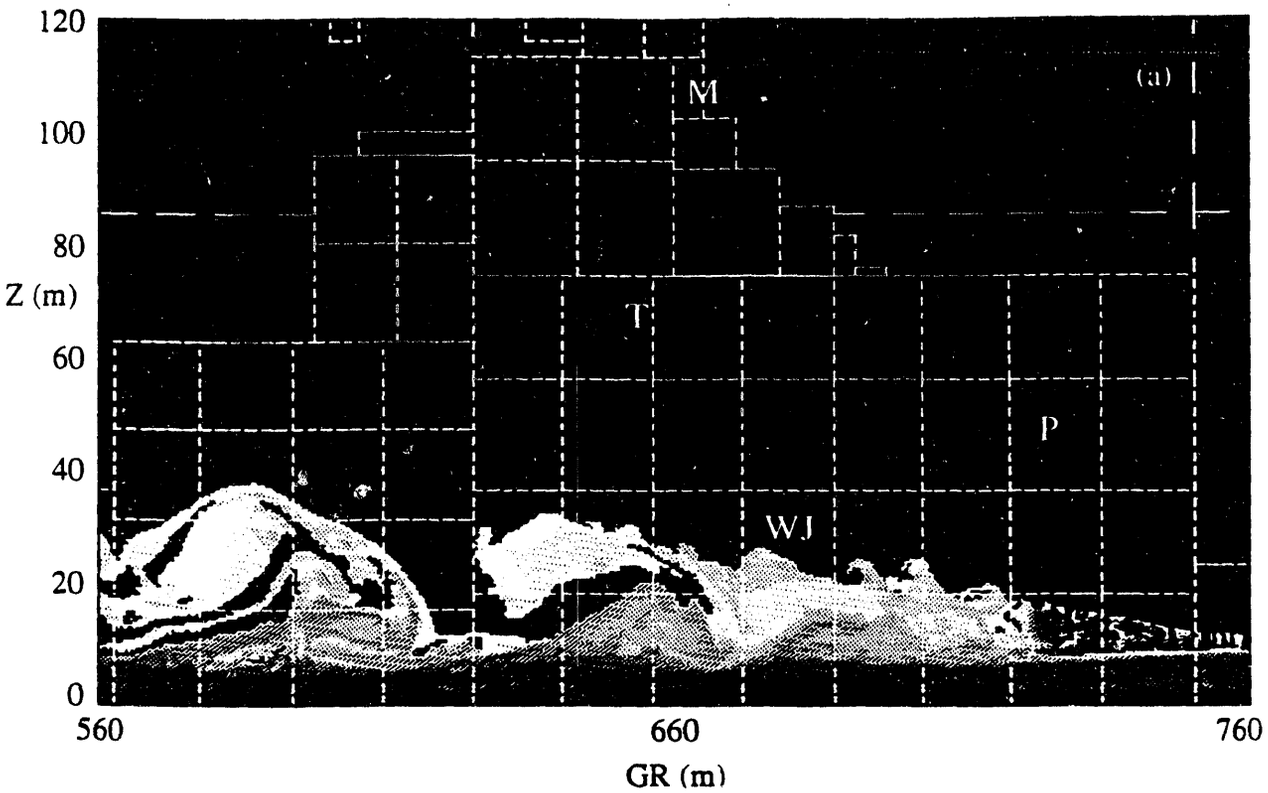

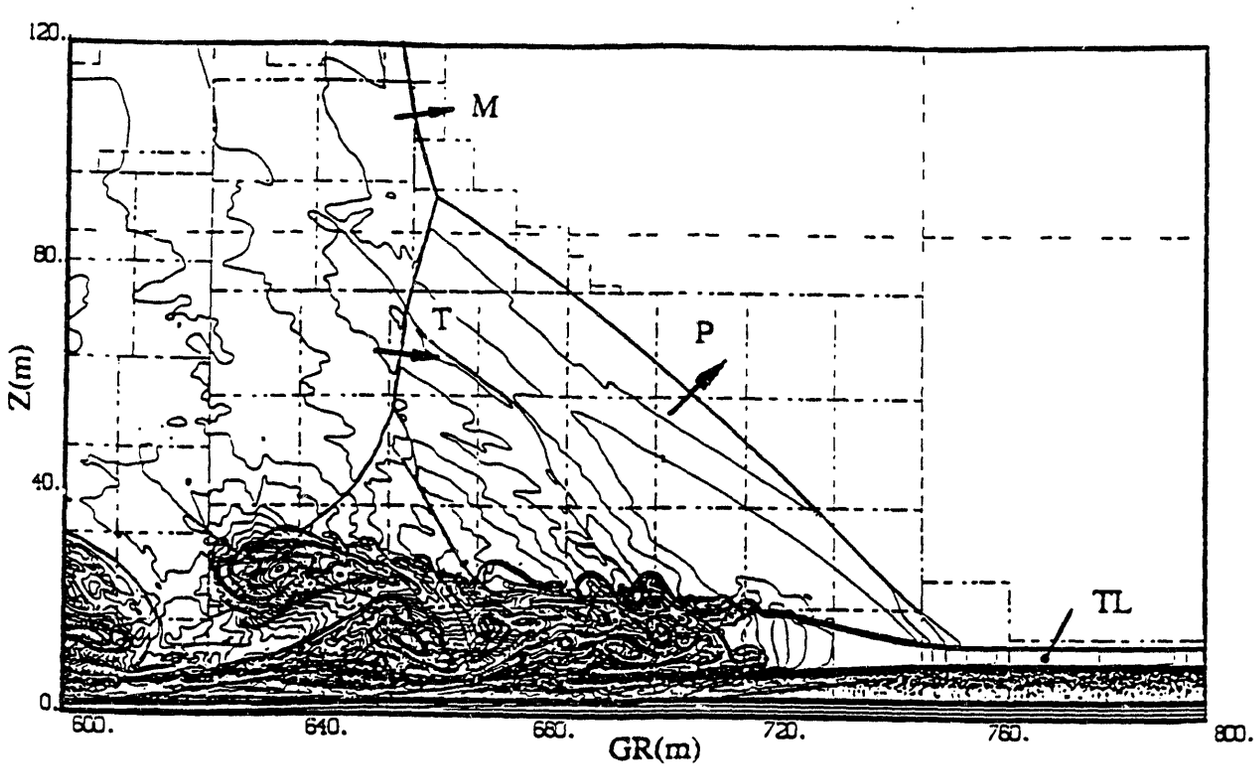

Figure 2. Cross-sectional view of the turbulent wall jet flow (t = 0.73 s).

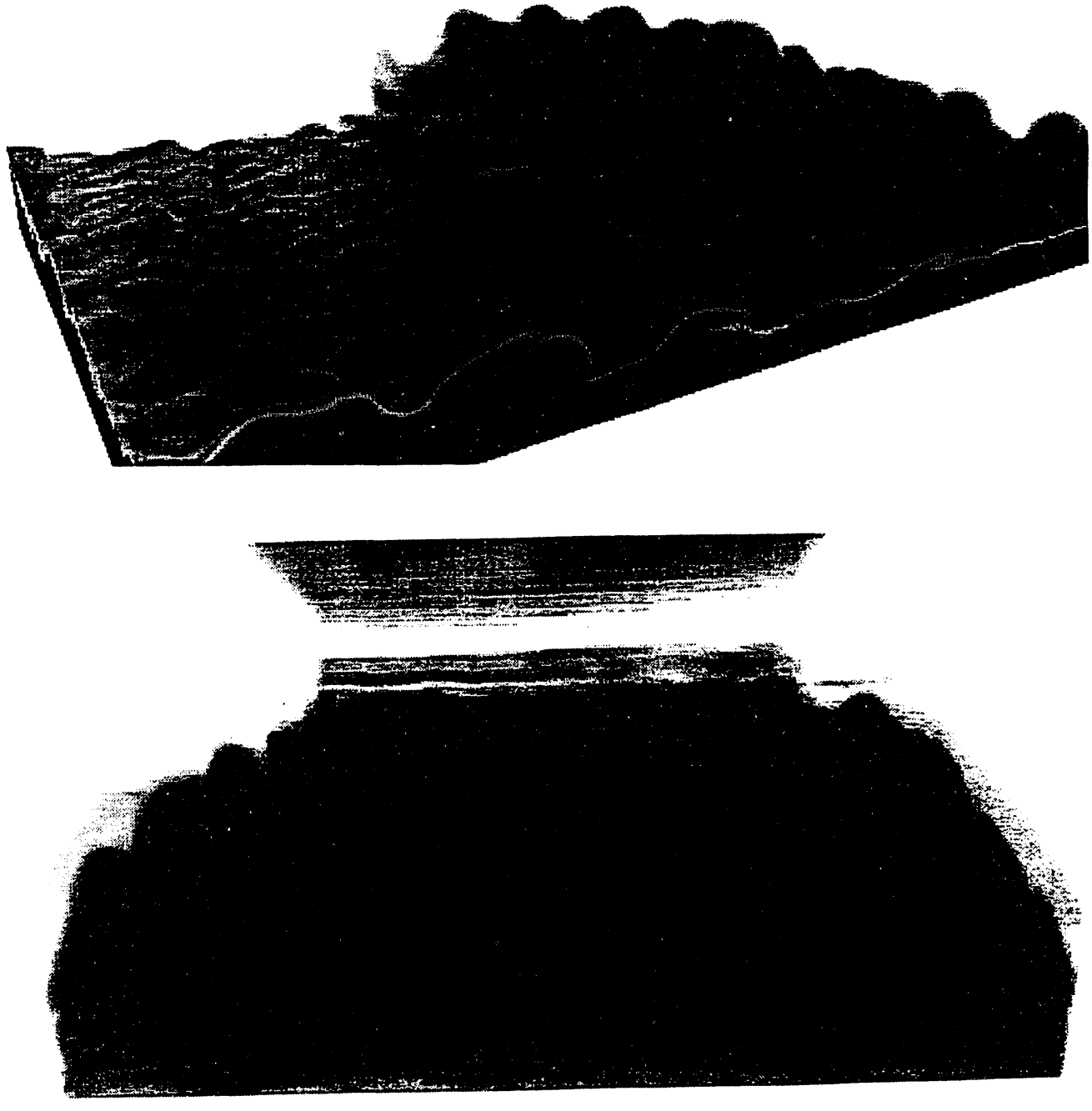

Figure 3. Three-dimensional visualization of the turbulent wall jet and dusty boundary layer flow at 1.68 s: (a) oblique view of the dust concentration; (b) vorticity magnitude, viewed looking toward ground zero.

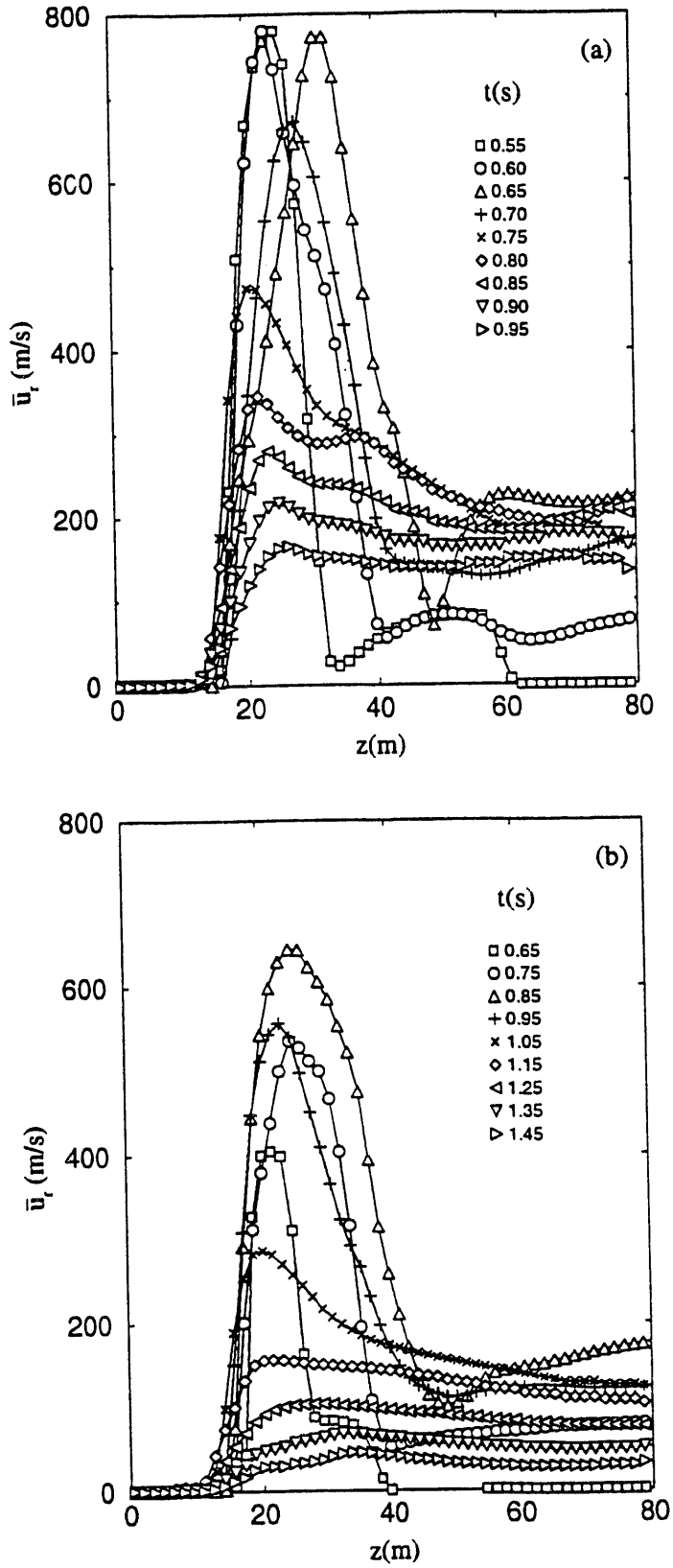

Figure 4. Evolution of the mean radial velocity profile versus time: (a) 600m; (b) 700m.

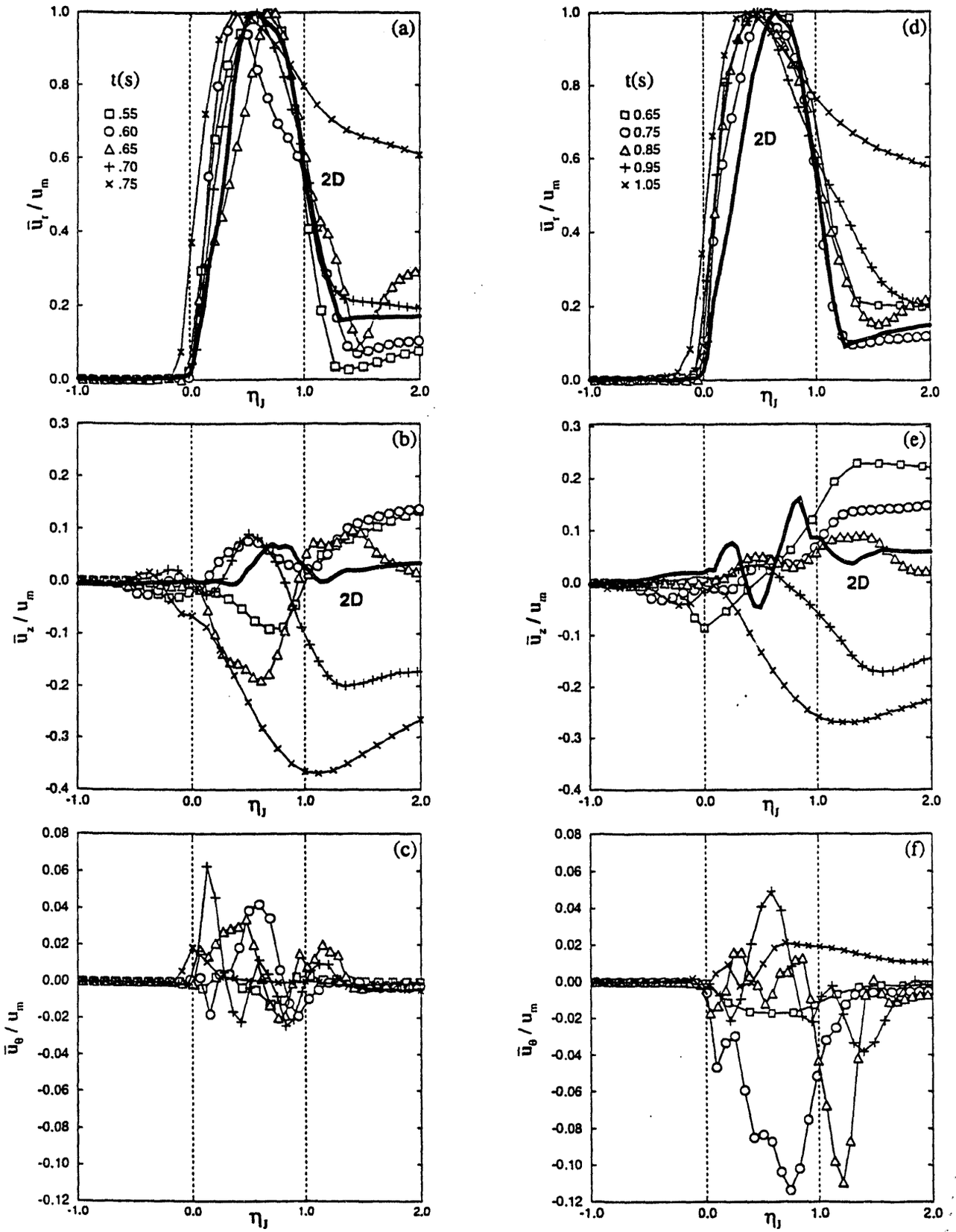

Figure 5. Mean velocity profiles in a precursor wall jet at 600m (a-radial, b-vertical, c-azimuthal) and 700m (d, e, f). Solid line denotes previous 2-D calculation (Kuhl et al., 1993).

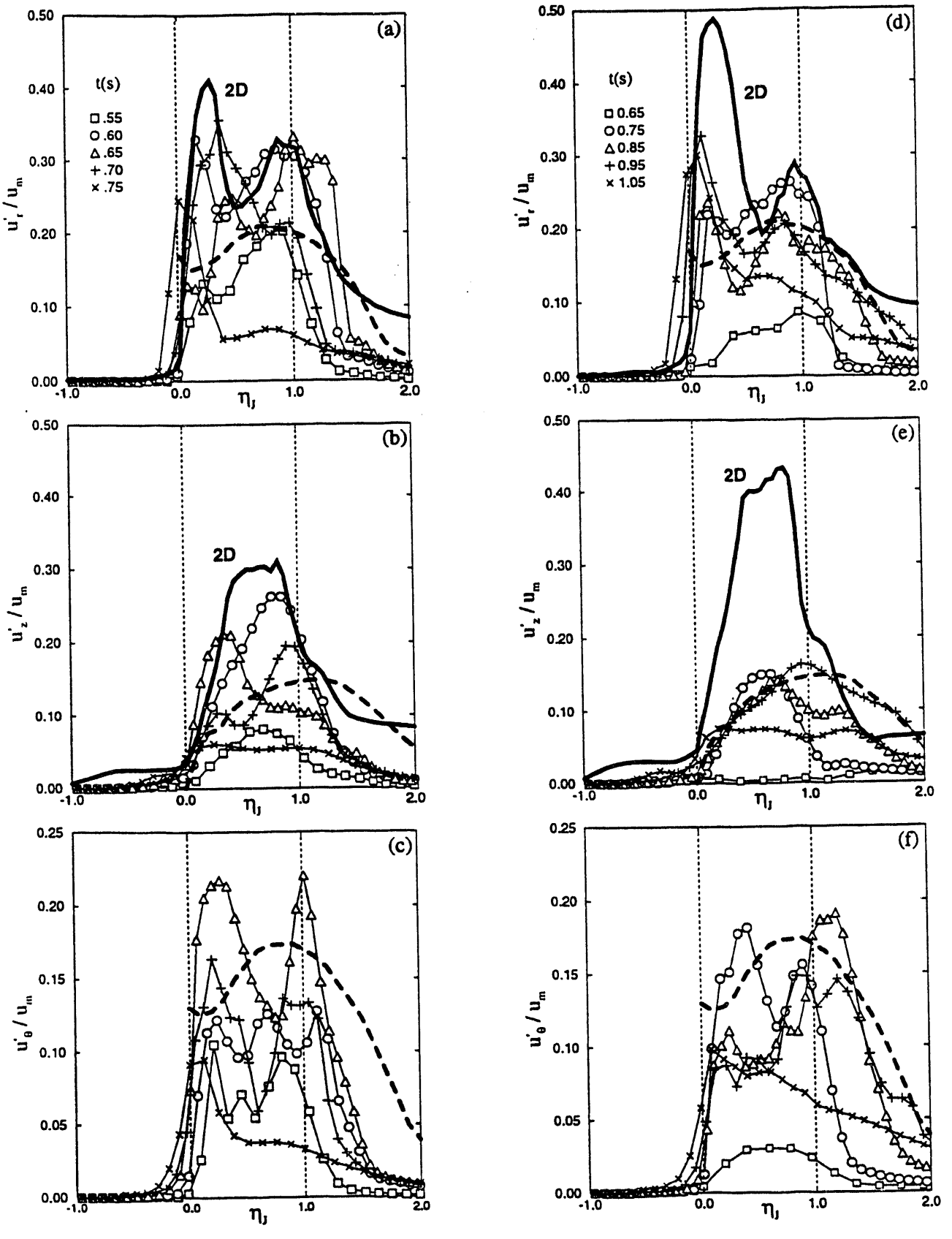

Figure 6. Velocity fluctuation profiles in a precursor wall jet at 600m (a-radial, b-vertical, c-azimuthal) and 700m (d, e, f). Solid line denotes previous 2-D calculation (Kuhl et al., 1993). Dashed lines denote measurements of a self-preserving 2-D clean wall jet (Launder and Rodi, 1981).

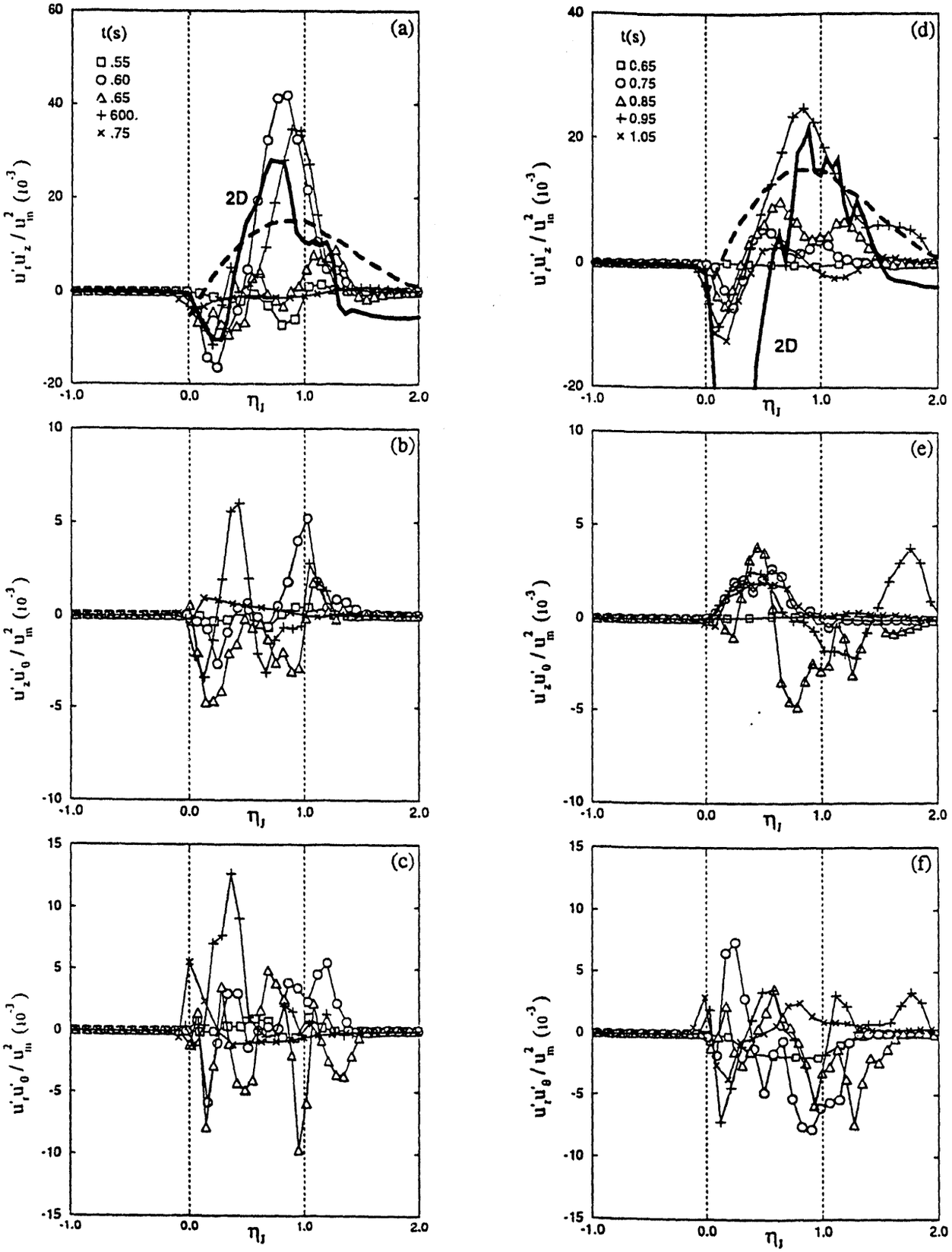

Figure 7. Reynolds stress profiles in a precursor wall jet at 600m (a-radial, b-vertical, c-azimuthal) and 700m (d, e, f). Solid line denotes previous 2-D calculation (Kuhl et al., 1993). Dashed lines denote measurements of a self-preserving 2-D clean wall jet (Launder and Rodi, 1981).

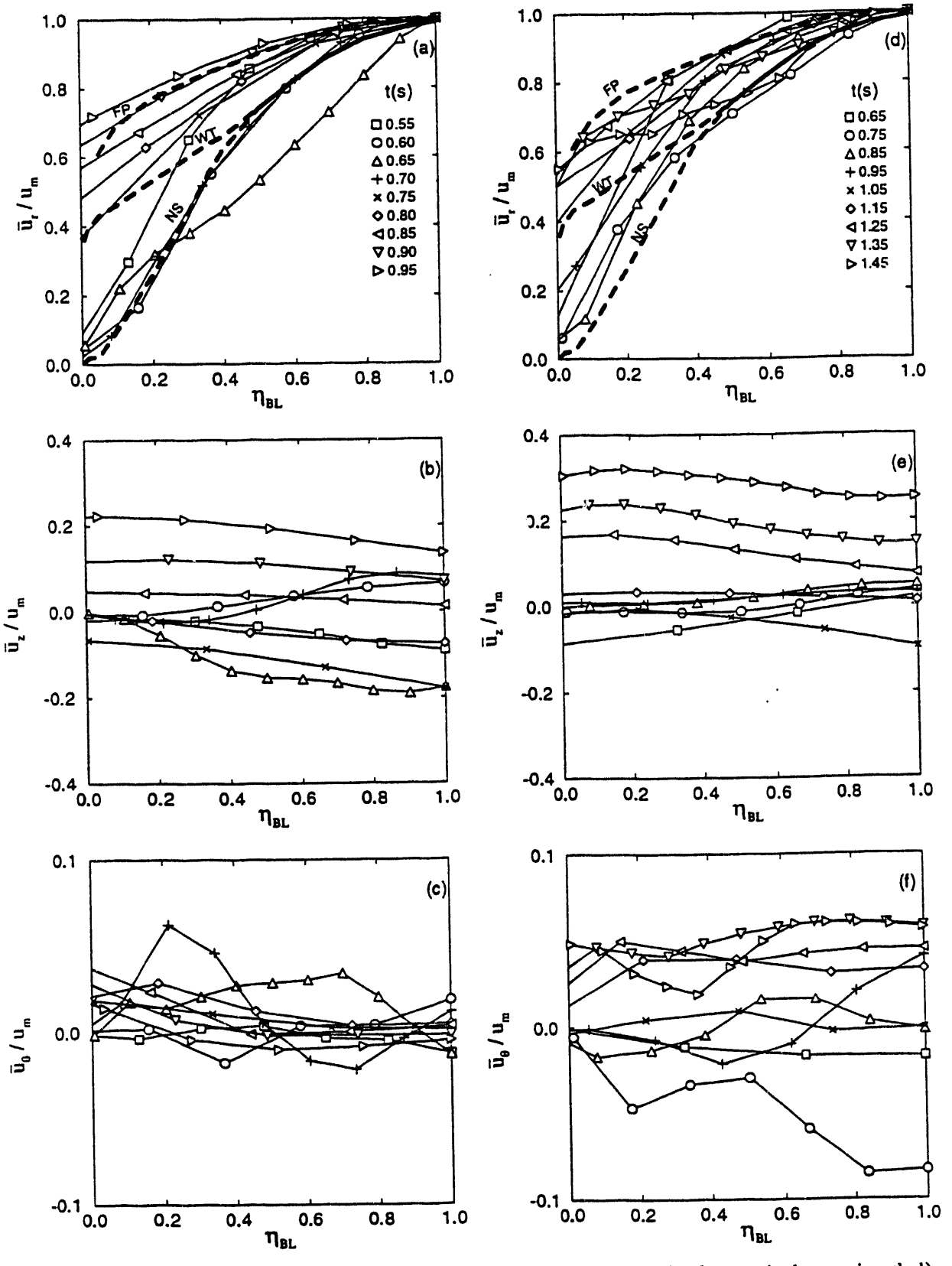

Figure 8. Mean velocity profiles in the boundary layer at 600 m (a - radial, b - vertical, c - azimuthal) and 700 m (d, e, f). Curves labeled NS and WT represent the dusty boundary layer profiles measured behind a normal shock (Batt et al., 1988) and in a wind tunnel (Batt et al., 1993), respectively, while curves labeled FP represent the turbulent boundary layer on a clean flat plate.

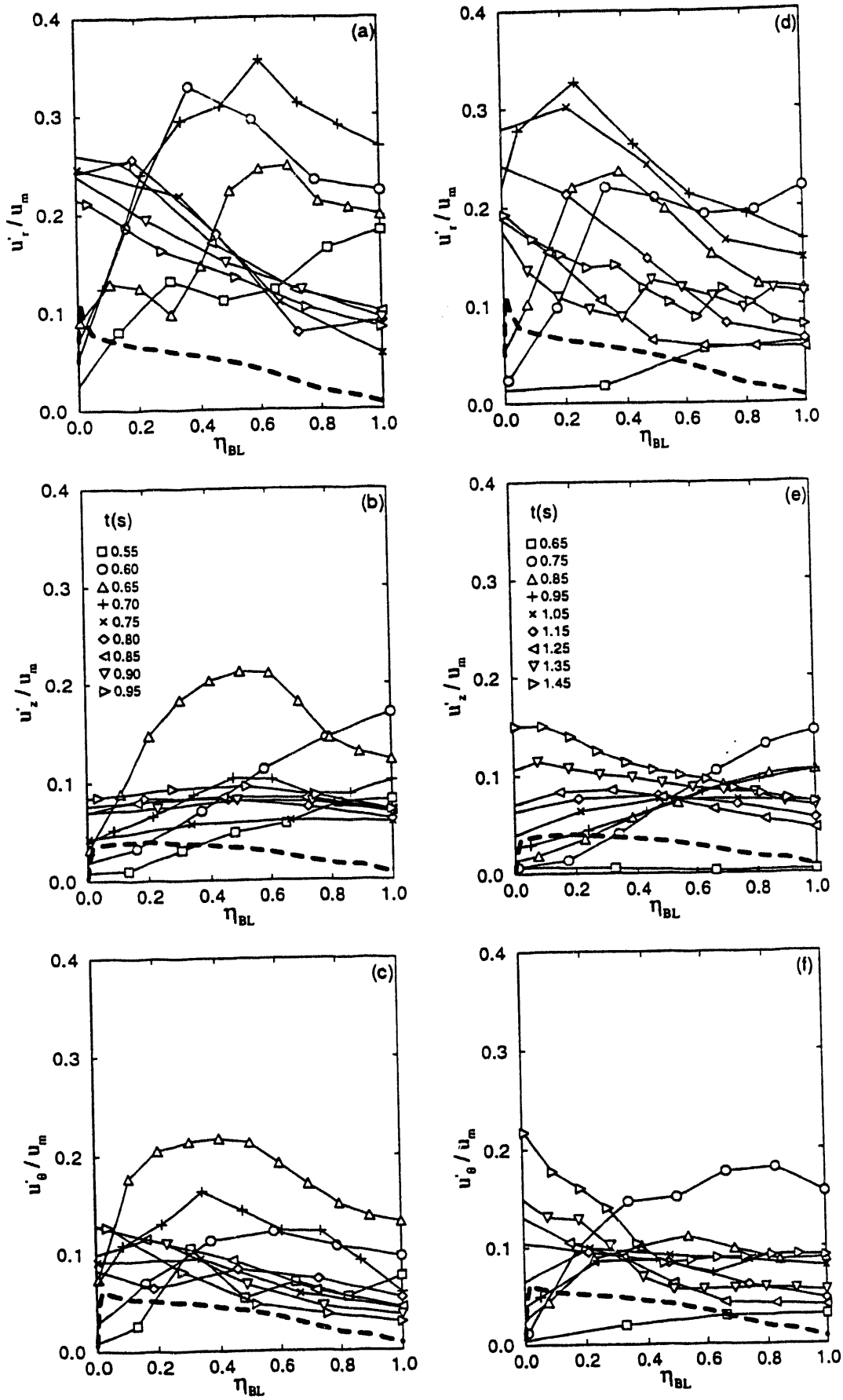

Figure 9. Velocity fluctuation profiles in the boundary layer at 600 m (a - radial, b - vertical, c - azimuthal) and 700 m (d, e, f). Dashed line represents measurements of a turbulent boundary layer on a clean flat plate (Klebanoff, 1955).

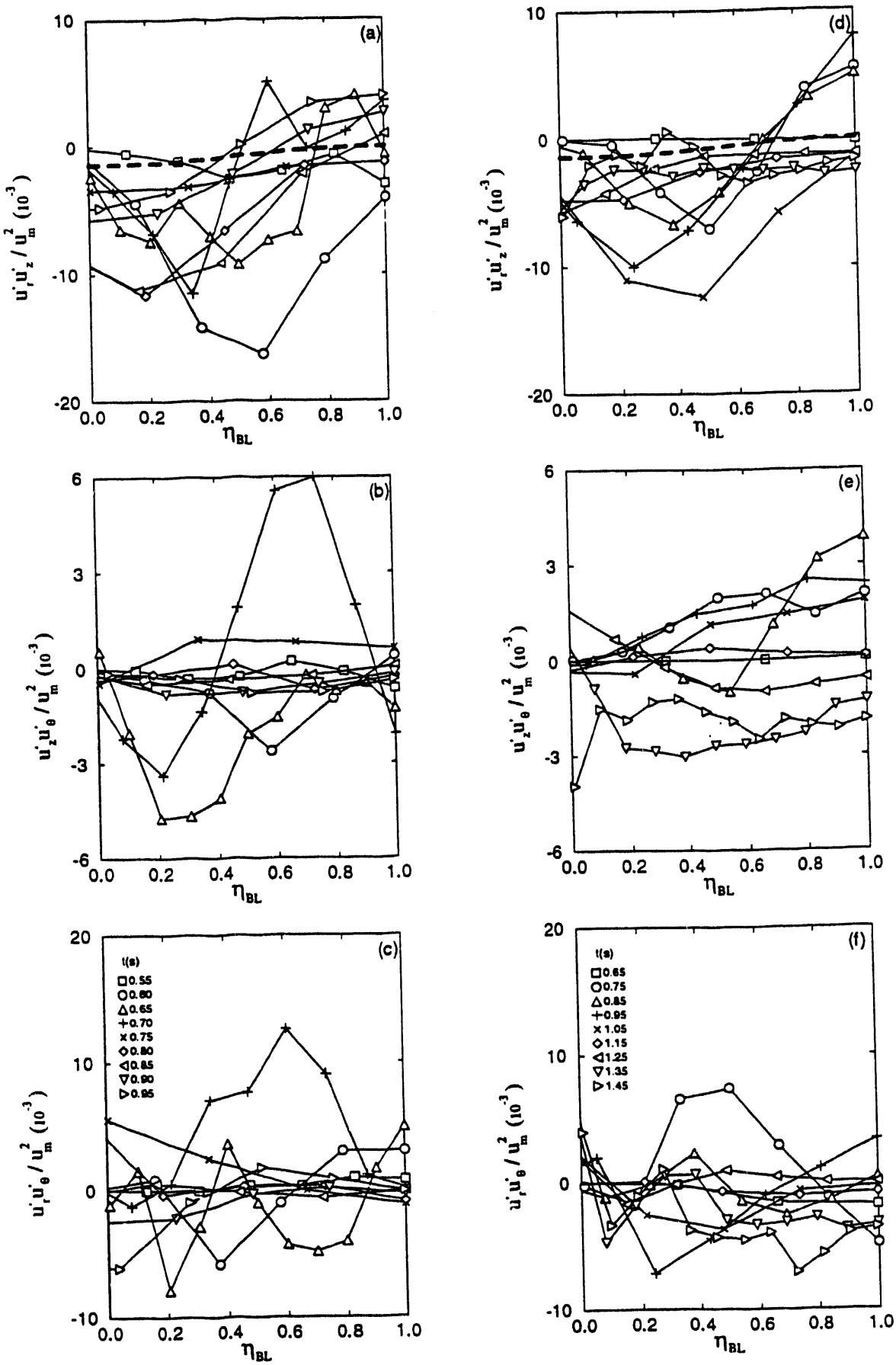

Figure 10. Reynolds stress profiles in the boundary layer at 600 m (a - radial, b - vertical, c - azimuthal) and 700 m (d, e, f). Dashed line represents measurements of a turbulent boundary layer on a clean flat plate (Klebanoff, 1955).

DATE
FILMED
6/30/94

END